Lagrangian Modeling, Linearization, and Optimal State-Feedback Control of a Nonlinear Inverted-Pendulum System

Dhiraj Basnet[1*]

[1*]Wahl Clipper Corporation, Sterling, 61081, IL, United States.

Corresponding author(s). E-mail(s): dhiraj.basnet@wahlclipper.com;

Abstract

This paper presents a simulation study of a cart–pole (inverted pendulum) system. Starting from first-principles physics, we derive the nonlinear equations of motion and linearize them about the upright equilibrium to obtain a state-space model for control design. Using this model, we synthesize an optimal Linear Quadratic Regulator (LQR) that balances regulation performance and control effort. All evaluations are performed in MATLAB/Simulink on the full nonlinear plant. Simulations show reliable recovery to the upright position with short settling time, limited overshoot, and negligible steady-state error. The workflow—modeling, linearization, and LQR design—is transparent and readily transferable to hardware.

Keywords: Control System, Optimal Control, State-Feedback, Linear Quadratic Regulator(LQR), Proportional-Integral-Derivative(PID), MATLAB, Center of Mass(COM), Euler-Lagrange.

1 Introduction

The inverted pendulum is a classic benchmark in control: easy to describe, hard to stabilize. A rigid pole on a moving cart has an upright equilibrium that is inherently unstable—small disturbances cause the pole to fall unless active control counteracts them. As a result, the system concentrates key challenges of practical control—nonlinearity, underactuation, tight timing, and limited actuation—while remaining compact enough for analysis and instruction.

A wide range of controllers including proportional–integral–derivative (PID) [1], [2], [3] optimal control [4], [5], [6], [7], and fuzzy control [8], [9], [10] can be implemented to stabilize the system. Historically, stabilization has often been attempted with heuristic methods, such as PID control tuned around a linearized model, root-locus pole placement, or gain scheduling across operating regions [11], [12], [13], [14]. These strategies can work for small disturbances and well-identified parameters, but tend to be sensitive to modeling errors, actuator limits, and large initial angles. In educational testbeds, one common practice is to first "swing up" the pendulum using energy-based reasoning and then hand-off to a locally tuned linear controller near the upright position.

In this paper, we follow a model-first, physics-guided route to stabilization and evaluate the approach entirely in simulation. We begin with a Lagrangian derivation of the coupled cart–pole dynamics, which makes the sources of nonlinearity (trigonometric coupling, gravity, and velocity-dependent terms) explicit. We then linearize about the upright equilibrium to obtain a compact state-space model suitable for analysis. On this foundation, we design an optimal state-feedback controller using Linear Quadratic Regulator (LQR). The LQR framework provides a systematic way to balance regulation speed against control effort.

All evaluations are performed in MATLAB/Simulink on the full nonlinear plant comparing open-loop and closed-loop responses. The simulations demonstrate rapid return to upright position, limited overshoot, and near-zero steady-state error across a range of scenarios, indicating that a straightforward LQR—grounded in a transparent physical model—can robustly stabilize the inverted pendulum.

2 System Dynamics

2.1 Geometry, coordinates, and modeling choices

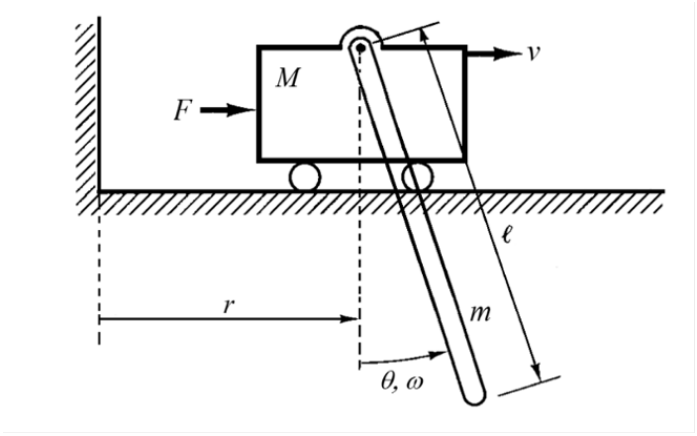

Fig. 1: Cart–pendulum geometry and variables.

We consider a cart of mass M that moves horizontally with position $r(t)$ (positive to the right) under input force $F(t)$ (Fig. 1). A uniform slender rod of mass m and length ℓ is pinned to the cart. The angle of the pendulum $\theta(t)$ is measured vertically downward: $\theta = 0$ is the hanging and $\theta = \pi$ is upright with gravity g acting downward. Dissipation is modeled by the viscous drag of the cart $\mu\dot{r}$ and the pivot torque $b\dot{\theta}$. Link compliance and wheel slip are neglected, whereas rolling resistance is determined in b. The Center of Mass (COM) of the rod lies at a distance $d = \ell/2$ from the pivot and its moment of inertia about the pivot is

$$I_p = \tfrac{1}{3} m \ell^2. \tag{1}$$

The generalized coordinates and velocities are represented as,

$$q = \begin{bmatrix} r \\ \theta \end{bmatrix}, \qquad \dot{q} = \begin{bmatrix} \dot{r} \\ \dot{\theta} \end{bmatrix}.$$

2.2 Kinematics and energies

The COM position and velocity is given as,

$$\begin{aligned} x_c &= r + d\sin\theta \\ y_c &= d\cos\theta \\ \dot{x}_c &= \dot{r} + d\cos\theta\,\dot{\theta} \\ \dot{y}_c &= -\,d\sin\theta\,\dot{\theta}. \end{aligned} \tag{2}$$

Hence

$$\dot{x}_c^{\,2} + \dot{y}_c^{\,2} = \dot{r}^{\,2} + 2d\cos\theta\,\dot{r}\,\dot{\theta} + d^2\dot{\theta}^{\,2}. \tag{3}$$

The kinetic and potential energies (zero at $\theta = 0$), and Rayleigh dissipation are given as,

$$T = \tfrac{1}{2}(M+m)\,\dot{r}^{\,2} + \tfrac{1}{2} I_p\,\dot{\theta}^{\,2} + md\cos\theta\,\dot{r}\,\dot{\theta}. \tag{4}$$

$$V = mgd\,(1-\cos\theta). \tag{5}$$

$$\mathcal{D} = \tfrac{1}{2}\mu\,\dot{r}^{\,2} + \tfrac{1}{2} b\,\dot{\theta}^{\,2}. \tag{6}$$

And the generalized forces including viscous terms are represented as,

$$\begin{aligned} Q_r &= F - \mu\,\dot{r} \\ Q_\theta &= -\,b\,\dot{\theta}. \end{aligned} \tag{7}$$

2.3 Euler-lagrange equations

With the Lagrangian $L = T - V$ and viscous dissipation, the forced Euler–Lagrange equations

$$\frac{d}{dt}\left(\frac{\partial L}{\partial \dot{q}_i}\right) \; - \; \frac{\partial L}{\partial q_i} \; = \; Q_i, \qquad i \in \{r, \theta\} \tag{8}$$

govern the coupled cart–pendulum dynamics under the generalized forces $Q_r = F - \mu \dot{r}$ (cart) and $Q_\theta = -b\dot{\theta}$ (pivot). Using the kinematics and energies derived earlier, we obtained the motion equations as,

$$\begin{gathered} (M+m)\,\ddot{r} \; + \; md\cos\theta\,\ddot{\theta} \; - \; md\sin\theta\,\dot{\theta}^2 \; = \; F \; - \; \mu\,\dot{r} \\ md\cos\theta\,\ddot{r} \; + \; I_p\,\ddot{\theta} \; + \; mgd\sin\theta \; = \; -\,b\,\dot{\theta}. \end{gathered} \tag{9}$$

With $d = \ell/2$, the compact matrix form is generated by grouping inertial, damping, gravity, velocity and input terms from (9) as,

$$\underbrace{\begin{bmatrix} \frac{1}{3}\,m\,\ell^2 & \frac{1}{2}\,m\,\ell\cos\theta \\ \frac{1}{2}\,m\,\ell\cos\theta & M+m \end{bmatrix}}_{H(\theta)} \begin{bmatrix} \ddot{\theta} \\ \ddot{r} \end{bmatrix} = \begin{bmatrix} -\frac{1}{2}\,m\,g\,\ell\sin\theta \; - \; b\,\dot{\theta} \\ \frac{1}{2}\,m\,\ell\,\dot{\theta}^2\sin\theta \; - \; \mu\,\dot{r} \; + \; F \end{bmatrix} \tag{10}$$

Similarly, the physical state form is represented by defining the states θ, $v = \dot{r}$ and $\omega = \dot{\theta}$ as,

$$\begin{gathered} \dot{\theta} = \omega \\ \begin{bmatrix} \dot{\omega} \\ \dot{v} \end{bmatrix} = H(\theta)^{-1} \begin{bmatrix} -\frac{1}{2}\,mg\ell\sin\theta \; - \; b\,\omega \\ \frac{1}{2}\,m\ell\sin\theta\,\omega^2 \; - \; \mu\,v \; + \; F \end{bmatrix} \end{gathered} \tag{11}$$

2.4 Normalization

Normalization simplifies analysis and simulation by reducing units, clustering parameters, and revealing intrinsic time scales. Based on the COM distance $d = l/2$, the natural frequency and normalized time are chosen as:

$$\omega_0 \; \triangleq \; \sqrt{\frac{g}{d}} \; = \; \sqrt{\frac{2g}{\ell}}, \qquad \tau \; = \; \omega_0 t.$$

The dimensionless states and input are defined as,

$$\omega \; = \; \frac{d\theta}{d\tau} \; = \; \frac{\dot{\theta}}{\omega_0}, \qquad v \; = \; \frac{\dot{r}}{\ell\,\omega_0}, \qquad F \; = \; \frac{F_{\dim}}{md\,\omega_0^2} \; = \; \frac{2F_{\dim}}{m\ell\,\omega_0^2},$$

and parameters as,

$$k = \frac{M}{m}, \qquad b_n = \frac{b}{md^2\omega_0} = \frac{4b}{m\ell^2\omega_0}, \qquad \mu_n = \frac{\mu}{m\omega_0}.$$

In further modeling, dots denote $d/d\tau$. And with an algebraic regrouping, the normalized compact form is represented as,

$$\begin{aligned} \dot{\theta} &= \omega \\ \begin{bmatrix} \dot{\omega} \\ \dot{v} \end{bmatrix} &= H_n(\theta)^{-1} \begin{bmatrix} -\sin\theta \;-\; 2b_n\,\omega \\ \frac{1}{2}\,\omega^2 \sin\theta \;+\; 2b_n\,\omega\cos\theta \;-\; \mu_n\,v \;+\; F \end{bmatrix} \end{aligned} \tag{12}$$

where,

$$H_n(\theta) = \begin{bmatrix} \frac{2}{3} & -\cos\theta \\ -\frac{1}{2}\cos\theta & k+1 \end{bmatrix}$$

The negative off-diagonal entries in $H_n(\theta)$ arise from measuring θ from the downward vertical with clockwise positive rotation. The term $-\sin\theta$ in the first RHS component is gravity about the pivot and the $2b_n\omega$ terms come from cart viscous drag carried through the coupling.
The nonlinear modeling of the inverted pendulum system expressed in (12) can also be represented in the form of explicit normalized ordinary differential equations.
Assuming $C = \cos\theta$, $S = \sin\theta$, the determinant of $H_n(\theta)$ can be calculated as,

$$\Delta(\theta) = \det H_n(\theta) = \frac{2}{3}(k+1) - \frac{1}{2}C^2.$$

This determinant is positive for typical lab parameters, ensuring $H_n(\theta)$ is invertible for all relevant θ. Then the inverse of $H_n(\theta)$ becomes,

$$H_n(\theta)^{-1} = \frac{1}{\Delta(\theta)} \begin{bmatrix} k+1 & C \\ \frac{1}{2}C & \frac{2}{3} \end{bmatrix}.$$

After substituting the value of $H_n(\theta)^{-1}$ in (12) and performing matrix multiplication, the normalized ODEs representing the dynamics of nonlinear pendulum cart system are,

$$\begin{aligned} \dot{\theta} &= \omega \\ \dot{\omega} &= \frac{(k+1)\big(-S - 2b_n\omega\big) \;+\; C\big(\frac{1}{2}\,\omega^2 S + 2b_n\omega C - \mu_n v + F\big)}{\Delta(\theta)} \\ \dot{v} &= \frac{\frac{1}{2}C\,\big(-S - 2b_n\omega\big) \;+\; \frac{2}{3}\big(\frac{1}{2}\,\omega^2 S + 2b_n\omega C - \mu_n v + F\big)}{\Delta(\theta)} \end{aligned} \tag{13}$$

3 Linearization and optimal control design

Having the full nonlinear state-space model in Section 2, we focus on local stabilization of the inverted equilibrium. For that, we linearized about the upright equilibrium

where the pendulum is balanced:

$$(\theta^\star, \omega^\star, v^\star, u^\star) = (\pi,\, 0,\, 0,\, 0), \qquad \sin\theta^\star = 0,\ \cos\theta^\star = -1.$$

At this point, the nonlinear velocity-dependent terms vanish and help to obtain A_π, B_π matrices, which capture the dominant small-signal behavior. These matrices enable a principled LQR design that trades off regulation performance and input effort, forming the foundation of robustness.

3.1 Linearization of nonlinear system

Let $\dot{x} = f(x,u)$ denote the normalized dynamics represented in (13). The linearized model about the upright is represented as,

$$\dot{\tilde{x}} = A_\pi\, \tilde{x} + B_\pi\, \tilde{u}, \qquad A_\pi = \left.\frac{\partial f}{\partial x}\right|_{(\theta^\star, u^\star)}, \quad B_\pi = \left.\frac{\partial f}{\partial u}\right|_{(\theta^\star, u^\star)},$$

with perturbations $\tilde{x} = x - x^\star$, $\tilde{u} = u - u^\star$.
Using $\dfrac{\partial}{\partial(\cdot)}\big(H_n^{-1}(\theta) g(x,u)\big) = H_n^{-1}\dfrac{\partial g}{\partial(\cdot)} - H_n^{-1}\Big(\dfrac{\partial H_n}{\partial\theta}\dfrac{\partial\theta}{\partial(\cdot)}\Big)H_n^{-1} g$ and the fact that $g(x^\star, u^\star) = 0$, and substituting $\sin\theta^\star = 0$, $\cos\theta^\star = -1$, we obtain the matrices as,

$$A_\pi = \begin{bmatrix} 0 & 1 & 0 \\ \dfrac{6(k+1)}{4k+1} & -\dfrac{12\, b_n (k+1)}{4k+1} & \dfrac{6\,\mu_n}{4k+1} \\ -\dfrac{3}{4k+1} & \dfrac{6\, b_n}{4k+1} & -\dfrac{4\,\mu_n}{4k+1} \end{bmatrix}, \qquad B_\pi = \begin{bmatrix} 0 \\ -\dfrac{6}{4k+1} \\ \dfrac{4}{4k+1} \end{bmatrix}.$$

Interpretation: The positive entry $A_\pi(2,1) > 0$ encodes the open-loop instability in the inverted configuration; the damping-related terms on $A_\pi(2,2)$ and $A_\pi(3,3)$ scale with b_n and μ_n; the off-diagonal damping/coupling entries $A_\pi(2,3)$ and $A_\pi(3,2)$ reflect translation–rotation coupling; and B_π shows how a cart force drives both angular acceleration and cart acceleration upright.

Controllability: For $k > 0$ and finite b_n, μ_n, the pair (A_π, B_π) is controllable, so full-state feedback can place the closed-loop poles arbitrarily.

3.2 Optimal LQR state-feedback design

After linearization around upright unstable equilibrium point, we design a continuous-time Linear–Quadratic Regulator for (A_π, B_π). Given $Q \succeq 0$ and $R \succ 0$, the cost function expressed as,

$$J \;=\; \int_0^\infty \big(x^\top Q x + u^\top R u\big)\, d\tau$$

is minimized by the linear feedback $u = -Kx$, with

$$K \;=\; R^{-1} B_\pi^\top P, \qquad A_\pi^\top P + P A_\pi - P B_\pi R^{-1} B_\pi^\top P + Q \;=\; 0,$$

where $P \succeq 0$ solves the continuous-time algebraic Riccati equation.

The values of the diagonal $Q = \text{diag}(q_\theta, q_\omega, q_v)$ and the scalar $R = r_u$ are the key parametrs for efficiently stabilizing the system via appropriate feedback gains K. The state weights Q are chosen to emphasize the response of certain states, while the control weight R is chosen to select how much control effort is used to solve the optimization problem.

4 Simulations, Results and Discussion

The simulation is carried out in MATLAB using the *ODE45* function and *Simulink* computation. For ease of simulation, the normalized parameters b_n, μ_n and k are assigned values of 0.05, 0.2 and 4 respectively.

4.1 Validation of the equations of motions

Initially, the dynamics of the system expressed in (13) is validated using a simple pendulum system approach. The rod is held at an angle of 0.8π and is released to swing, where π represents the upright position relative to the initial downward position. Fig. 2 shows the position (θ), angular velocity (ω) of the rod, and linear velocity (v) of the cart against time.

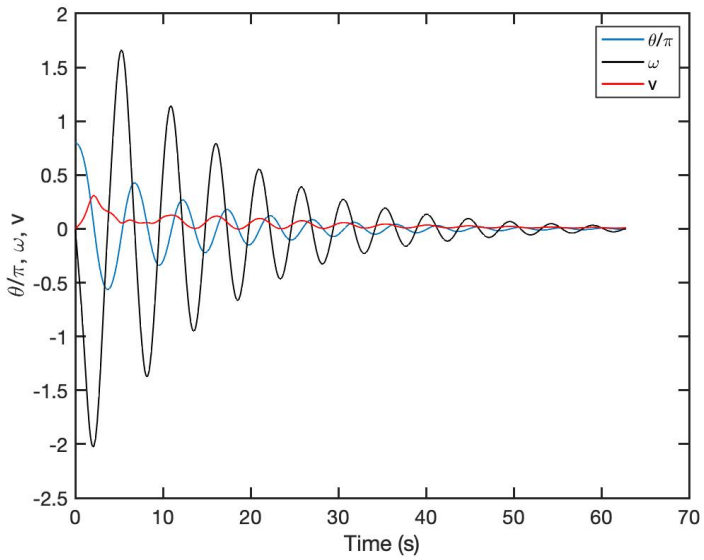

Fig. 2: Inverted pendulum states vs. time without application of controller. Angle is plotted as θ/π (so 1 corresponds to the upright position, $\theta = \pi$ rad); ω in rad/s; cart velocity v in m/s.

Fig. 2 shows that in normal condition, when the pendulum is dropped from a certain angle then the state variables decay by time and eventually settle to zero. This behavior is consistent with the model assumptions and supports the correctness of the derived equations.

4.2 Instability of the lineraized system

The linearized system remains unstable. The instability of the system is illustrated by using the pole location technique. With the normalized parameter values, the matrices A_π and B_π are computed as,

$$A_\pi = \begin{bmatrix} 0 & 1 & 0 \\ 1.765 & -0.177 & 0.071 \\ -0.176 & 0.018 & -0.047 \end{bmatrix}, \qquad B_\pi = \begin{bmatrix} 0 \\ -0.353 \\ 0.235 \end{bmatrix}.$$

The poles are obtained by getting the eigen values using the function *eig(A)* and are -1.416, 1.246 and -0.054. Because one eigenvalue lies in the right-half plane, the linearized system is unstable, motivating the feedback design.

4.3 Controllability

Before designing the controller, the linearized system is checked for its controllability via it's rank and comparing it with state variables and order of the system. The rank is determined to be 3 using *rank(ctrb(A,B))* function. Similarly, the transfer function of the system is calculated using *sstf* and *tf* functions and expressed as,

$$G(s) = \frac{-0.353\,s - 0.03328}{s^3 + 0.224\,s^2 - 1.755\,s - 0.09545}. \tag{14}$$

The order of the transfer function is 3 and the rank is also 3. So, the proposed linearized system is controllable, and the optimal controller can be designed for it.

4.4 LQR state-feedback and control tuning

To convert the open-loop system to closed loop, state-feedback approach is used such that the input to the system is updated with respect to the state variables as,

$u(t) = -Kx(t)$.

The appropriate value of K determines the shifting of eigen values of unstable system to left-half plane.

Linear Quadratic Regulator (LQR) Control technique is used to determine the optimum values of K. LQR provides a principled trade-off between state regulation (via Q) and control effort (via R), and yields a unique stabilzing gain K from the solution of the continuous-time algebraic Riccati equation. The state weight Q and control

weight R are chosen as,

$$Q = \begin{bmatrix} 150 & 0 & 0 \\ 0 & 50 & 0 \\ 0 & 0 & 30 \end{bmatrix}, \qquad R = 0.001$$

Using these weights and function $LQR(A, B, Q, R)$, the feedback gains are calculated as

$$K = \begin{bmatrix} -516.335 & -342.505 & -128.568 \end{bmatrix}$$

With these feedback gains in use, the poles of the system are calculated again using function $eig(A - B * K)$, and found to be -88.813, -1.685 and -0.417. This shows that all the poles are located in the left-half plane, so the system has turned to be stable. The LQR controller has done its duty perfectly by allocating the eigen values in the correct position to stabilize the system.

4.5 Closed-loop nonlinear simulation

The feedback gains K update the state variables according to the input and set point. The set point for the proposed inverted pendulum system is π which is upright position. With this set point, the LQR controller is applied to the original nonlinear system in (13) and it's response is observed as shown in Fig. 3,

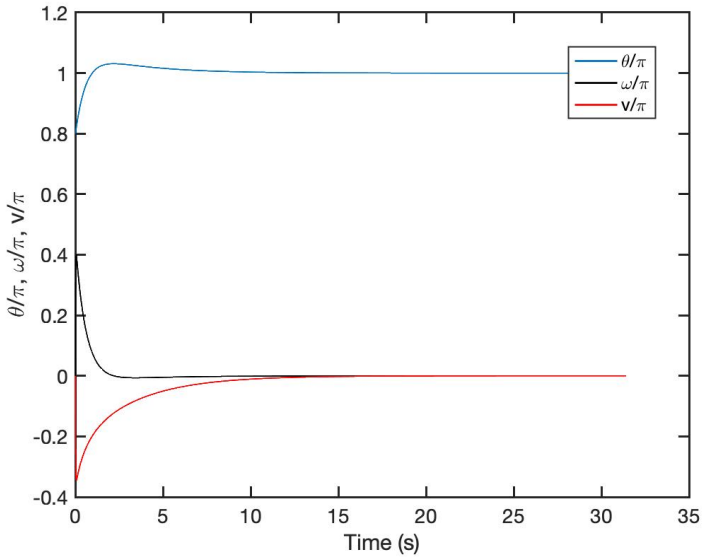

Fig. 3: Inverted pendulum states vs. time with application of controller. Angle is plotted as θ/π (so 1 corresponds to the upright position, $\theta = \pi$ rad); ω in rad/s; cart velocity v in m/s.

Fig. 3 shows that the controller efficiently stabilized the inverted pendulum in the upright position, having an initial starting point of 0.8π. Similarly, the angular velocity ω and the linear velocity v are also stabilized at 0. Furthermore, the controller is capable of keeping the transient response short with almost zero steady-state error.

4.6 Simulink implementation

The dynamical modeling of the system is validated using Simulink, also. Initially, the behavior of the system is observed without the controller and having the pendulum released from an angle of 0.8π. The Simulink model and the graphical response for it are shown in Fig. 4 and Fig. 5, respectively.

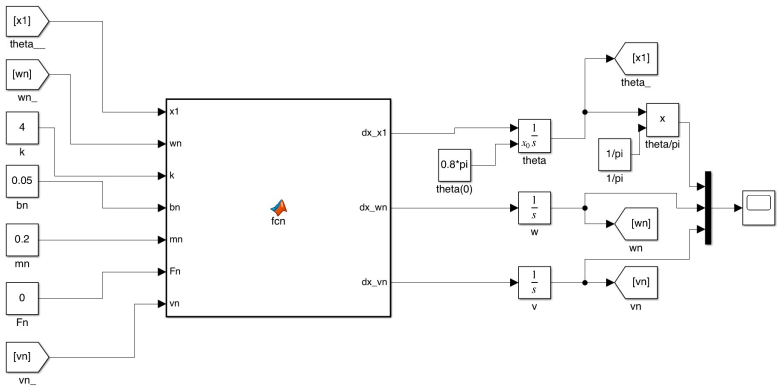

Fig. 4: Simulink block diagram of the inverted pendulum cart system without application of controller.

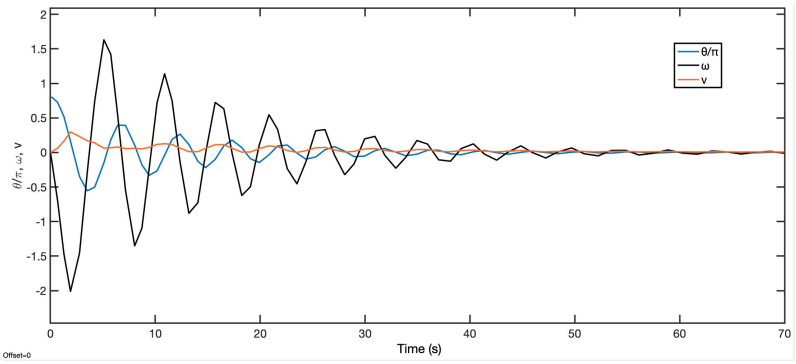

Fig. 5: Inverted pendulum states vs. time without application of controller, modeled in Simulink. Angle is plotted as θ/π (so 1 corresponds to the upright position, $\theta = \pi$ rad); ω in rad/s; cart velocity v in m/s.

Fig. 5 shows that the pendulum rod when released from an angle of 0.8π, decays by time and ultimately settles down to rest position i.e. vertically downward. This validates the correctness of the mathematical modeling of the inverted pendulum cart system from Simulink environment too.

Similarly, the behaviour of the system is also observed in response to the applied LQR controller. The Simulink model to showcase application of controller and system's response are shown in Fig. 6 and Fig. 7 respectively.

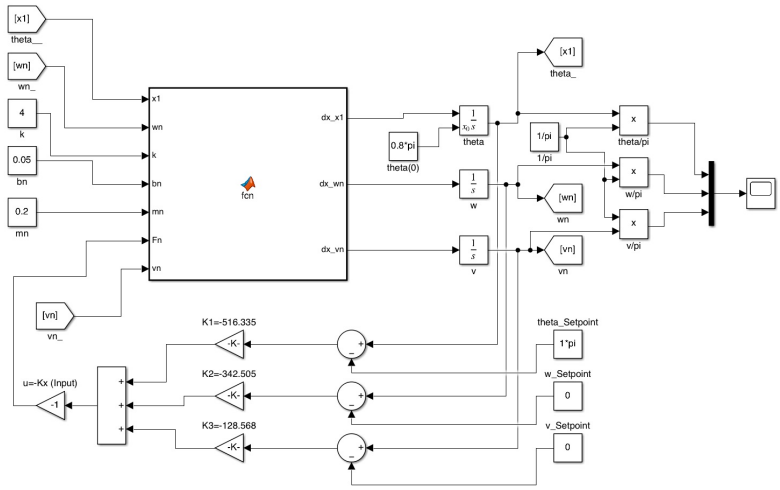

Fig. 6: Simulink block diagram of the inverted pendulum cart system with application of controller.

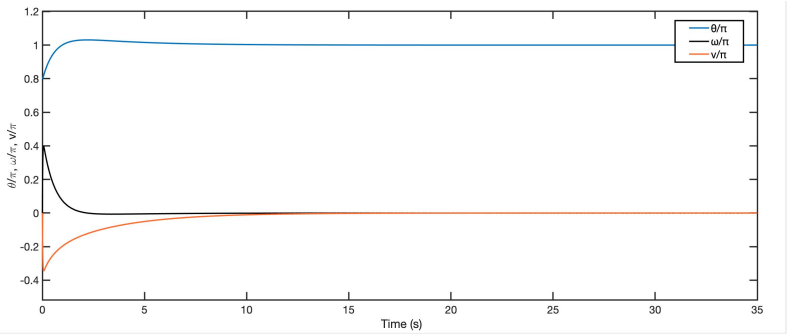

Fig. 7: Inverted pendulum states vs. time with application of controller, modeled in Simulink. Angle is plotted as θ/π (so 1 corresponds to the upright position, $\theta = \pi$ rad); ω in rad/s; cart velocity v in m/s.

Fig. 7 shows that the LQR controller has efficiently stabilized the pendulum in an upright position by adjusting the input with respect to the change in state variables.

5 Conclusion

This work presented a complete simulation-based workflow for stabilizing the cart–pendulum system: a clear angle convention, Lagrangian modeling, a compact normalized state–space form with $H_n(\theta)$, linearization at the upright equilibrium, and an optimal LQR design. The resulting controller reliably stabilized the inverted configuration on the full nonlinear model, meeting standard performance metrics. Although evaluated in simulation, normalization and closed-form (A_π, B_π) make the method directly transferable to hardware. Future work will integrate swing-up, output-feedback/observer design, and constraint handling (e.g., MPC) to broaden operating range and robustness.

References

[1] Jiang, H.: Overview and development of pid control. Applied and Computational Engineering **66**, 187–191 (2024) https://doi.org/10.54254/2755-2721/66/20240946

[2] Basnet, D., Lamichhane, A., Panthi, A., Lamichhane, B., Badrudoza, M., Pandey, R.: Controlled position navigation of single degree magnetic levitation. Proceeding of the Electrical Engineering Computer Science and Informatics **6** (2019) https://doi.org/10.11591/eecsi.v6.2016

[3] Hägglund, T., Guzmán, J.L.: Give us pid controllers and we can control the world**this work has been financed by the following projects: Pid2020–112709rb-c21 project financed by the spanish ministry of science. IFAC-PapersOnLine **58**(7), 103–108 (2024) https://doi.org/10.1016/j.ifacol.2024.08.018 . 4th IFAC Conference on Advances in Proportional-Integral-Derivate Control PID 2024

[4] Locatelli, A.A., Sieniutycz, S.R.: Optimal control: An introduction. Applied Mechanics Reviews **55**(3), 48–49 (2002) https://doi.org/10.1115/1.1470675 https://asmedigitalcollection.asme.org/appliedmechanicsreviews/article-pdf/55/3/B48/5438787/b41$_1$.*pdf*

[5] Basnet, D.: Design, implementation, and feedback stabilization of a permanent magnet levitation system. Master's thesis, Southern Illinois University Carbondale, Carbondale, IL, USA (2023). https://opensiuc.lib.siu.edu/theses/3114/

[6] Basnet, D., Komaee, A.: Magnetic levitation using permanent magnets: System design, feedback stabilization, and experimental validation. In: 2024 IEEE International Conference on Advanced Intelligent Mechatronics (AIM), pp. 237–242 (2024). https://doi.org/10.1109/AIM55361.2024.10637103

[7] Chen, W.-H., Ballance, D.J., Gawthrop, P.J.: Optimal control of nonlinear systems: a predictive control approach. Automatica **39**(4), 633–641 (2003) https://doi.org/10.1016/S0005-1098(02)00272-8

[8] Tanaka, K., Sugeno, M.: Stability analysis and design of fuzzy control systems. Fuzzy Sets and Systems **45**(2), 135–156 (1992) https://doi.org/10.1016/0165-0114(92)90113-I

[9] Nguyen, A.-T., Taniguchi, T., Eciolaza, L., Campos, V., Palhares, R., Sugeno, M.: Fuzzy control systems: Past, present and future. IEEE Computational Intelligence Magazine **14**(1), 56–68 (2019) https://doi.org/10.1109/MCI.2018.2881644

[10] Tanaka, K., Hori, T., Wang, H.O.: A fuzzy lyapunov approach to fuzzy control system design. In: Proceedings of the 2001 American Control Conference. (Cat. No.01CH37148), vol. 6, pp. 4790–47956 (2001). https://doi.org/10.1109/ACC.2001.945740

[11] Kumar, V., Agarwal, R.: Modeling and control of inverted pendulum cart system using pid-lqr based modern controller. In: 2022 IEEE Students Conference on Engineering and Systems (SCES), pp. 01–05 (2022). https://doi.org/10.1109/SCES55490.2022.9887706

[12] Duan, L., Su, X., Tang, Y., Yang, H., Zhang, H.: Application of pid tracking control in inverted pendulum system. In: 2021 IEEE 4th Advanced Information Management, Communicates, Electronic and Automation Control Conference (IMCEC), vol. 4, pp. 1815–1819 (2021). https://doi.org/10.1109/IMCEC51613.2021.9482036

[13] M, A.L., Kunjumuhammed, A., Tomy, J., G, U., Sivadas, M., Mohan, A.: Stabilization of rotary inverted pendulum using pid controller. In: 2021 8th International Conference on Smart Computing and Communications (ICSCC), pp. 376–380 (2021). https://doi.org/10.1109/ICSCC51209.2021.9528290

[14] Omatu, S., Fujinaka, T., Yoshioka, M.: Neuro-pid control for inverted single and double pendulums. In: Smc 2000 Conference Proceedings. 2000 Ieee International Conference on Systems, Man and Cybernetics. 'cybernetics Evolving to Systems, Humans, Organizations, and Their Complex Interactions' (cat. No.0, vol. 4, pp. 2685–26904 (2000). https://doi.org/10.1109/ICSMC.2000.884401